

Regge Poles and $SU(3)$: Particle Classification and High-Energy Scattering*†

V. BARGER

Department of Physics, University of Wisconsin, Madison, Wisconsin

An integrated interpretation of the fundamental particle spectrum and the phenomena observed in high-energy scattering is possible within the framework provided by the $SU(3)$ and Regge pole theories of strong interactions. Recent progress in this direction is reviewed with particular emphasis on qualitative predictions and experimental tests. The presence of forward and backward peaks in scattering angular distributions is associated with the existence of certain $SU(3)$ multiplets of mesons and baryons that mediate the reactions as peripheral exchanges. The observed baryons are tentatively classified as Regge recurrences of 1-, 8-, and 10-dimensional $SU(3)$ multiplets. For mesons, recurrences of only 1 and 8 representations are expected. Predictions for charge-exchange processes based on meson Regge exchanges are described in some detail. $SU(3)$ symmetry for the vertices of the Regge exchanges leads to relations that agree with experiment. Scattering in the intermediate momentum range (1–4 BeV/c) is described in terms of an interference model which incorporates direct channel resonances as well as Regge exchange. Structure in forward $\pi^-p \rightarrow \pi^0n$ scattering and backward π^-p elastic scattering is interpreted by interference model calculations.

I. INTRODUCTION

The scattering of fundamental particles at high energy has revealed the existence of an enormous number of resonance states. Along with the discovery of these resonance particles has come a wealth of experimental information regarding the energy and angular dependence of both elastic and inelastic scattering processes. Recent applications suggest that peripheral models based on Regge poles and $SU(3)$ may describe an appreciable fraction of the scattering data. At the same time these theories potentially provide a framework for classification of the numerous particles. In this article some of the encouraging prospects of a $SU(3)$ -Regge pole description of particle classification and high-energy scattering are discussed.

The application of Regge poles to scattering is made in the spirit of the usual peripheral model. The scattering amplitude at high energy is assumed to be dominated by a limited number of peripheral exchanges (Fig. 1). For concreteness let us consider pseudoscalar meson-spin $\frac{1}{2}$ baryon scattering. The center-of-mass scattering angle is always defined to be the angle between the incident and outgoing mesons. For small angle scattering ($\cos \theta_{c.m.} \simeq +1$) the dominant mechanism is meson exchange which causes sharp forward peaking of the differential cross section. At the other extreme baryon exchange gives rise to a rather sharp backward peak ($\cos \theta_{c.m.} \simeq -1$) in angular distributions. At intermediate energies, the presence of direct channel resonances can somewhat complicate the simple features of the peripheral exchanges.

* Work supported, in part, by the University of Wisconsin Research Committee with funds granted by the Wisconsin Alumni Research Foundation, and, in part, by the U.S. Atomic Energy Commission under Contract AT(11-1)-881, COO-881-112.

† This article is based on a talk presented at the Washington meeting of the American Physical Society on 25 April 1967.

In the pseudoscalar meson-spin $\frac{1}{2}$ baryon scattering example, the external mesons and baryons are members of octet representations of $SU(3)$. Consequently, the mesons or baryons which can be exchanged belong to

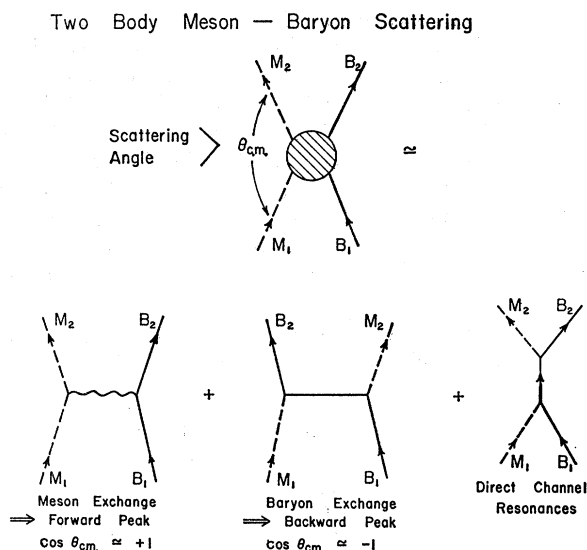


FIG. 1. Illustration of peripheral meson and baryon exchange approximation to the scattering amplitude at high energy. Direct channel resonance effects also make important contributions at intermediate energies.

either 1, 8, 10, $\bar{10}$, or 27 representations. The presence or absence of peripheral peaks in the scattering angular distributions bears directly on which of these $SU(3)$ representations of particles are exchanged—and hence which $SU(3)$ multiplets of particles occur in nature. In order to obtain such information, let us examine some representative experimental data at laboratory momenta of 3 BeV/c.

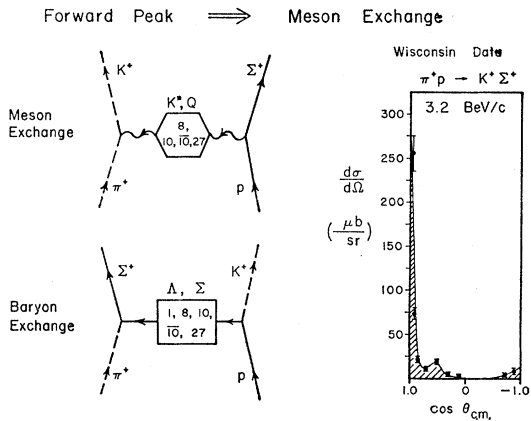


FIG. 2. Forward and backward peaks in the reaction $\pi^+p \rightarrow K^+\Sigma^+$. Schematic diagrams indicate the possible $SU(3)$ representations for the meson and baryon exchanges. [Data from R. R. Kofler, R. W. Hartung, and D. D. Reeder, Phys. Rev. (to be published).]

II. EXPERIMENTAL EVIDENCE ON PERIPHERAL SCATTERING

The reaction $\pi^+p \rightarrow K^+\Sigma^+$ is representative of processes involving both meson and baryon exchange (Fig. 2). The boxes in the schematic exchange diagrams of Fig. 2 indicate the possible $SU(3)$ representations that can mediate the reaction. The data show a forward peak of $\sim 250 \mu\text{b}/\text{sr}$ and a backward peak of $\sim 10 \mu\text{b}/\text{sr}$. Forward peaks are typically more than an order of magnitude higher than backward peaks. In the reaction $K^-p \rightarrow \bar{K}^0n$ (Fig. 3) a sharp forward peak is again present, but no events are observed near $\cos \theta_{\text{c.m.}} \simeq -1$. The absence of a backward peak here can be interpreted as evidence against baryons in $\bar{10}$ or 27 $SU(3)$ representations.

The distinct features of a baryon exchange peak are more clearly illustrated by the data on the reaction

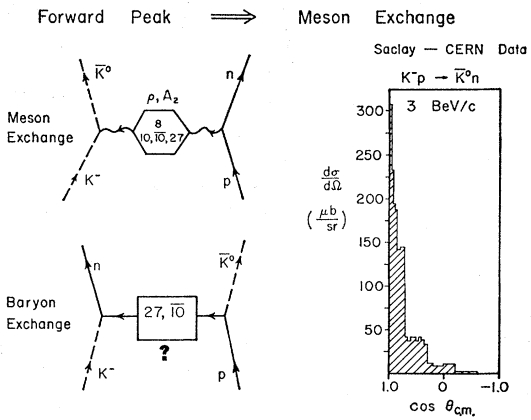


FIG. 3. Absence of a backward peak in $K^-p \rightarrow \bar{K}^0n$ provides evidence against $\bar{10}$ and 27 baryon multiplet exchanges. [Data from J. Badier *et al.*, Saclay Report (1966).]

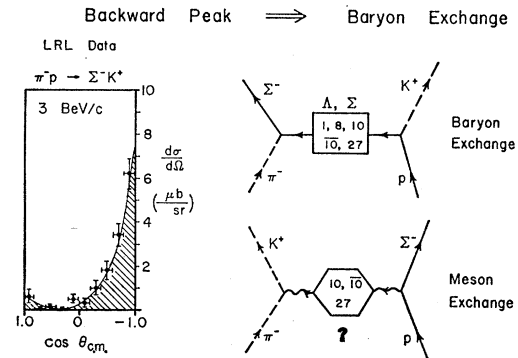


FIG. 4. Distinct features of a baryon exchange peak are revealed by the reaction $\pi^-p \rightarrow \Sigma^-K^+$. The absence of 10, $\bar{10}$, or 27 meson multiplet exchanges is inferred from the scattering angular distribution. [Data from O. I. Dahl *et al.*, UCRL Report 17217 (1967).]

$\pi^-p \rightarrow \Sigma^-K^+$ (Fig. 4). The backward peak is of the expected order of magnitude $\sim 8 \mu\text{b}/\text{sr}$, and there is a notable absence of events near $\cos \theta_{\text{c.m.}} \simeq +1$. The absence of a forward peak is interpreted as evidence against 10, $\bar{10}$, or 27 $SU(3)$ meson multiplets. A similar interpretation of the angular distribution of the reaction $K^-p \rightarrow \Xi^-K^+$ (Fig. 5), which again has only the backward peak, also eliminates possible meson exchanges of 27-dimensional $SU(3)$ representations.

Such inferences are by no means limited to inelastic reactions. In elastic scattering at backward angles (Fig. 6), the differential cross section for K^-p scattering is at least an order of magnitude smaller than the corresponding measurements for K^+p or $\pi^\pm p$ elastic scattering. As before, we draw the conclusion that no 27 baryon multiplets are exchanged.

To summarize these conclusions no forward peaks in $\pi^-p \rightarrow \Sigma^-K^+$ and $K^-p \rightarrow K^+\Xi^-$ implies no meson exchanges of 10, $\bar{10}$, or 27 $SU(3)$ multiplets, whereas no backward peaks in $K^-p \rightarrow p\bar{K}^-$ and $K^-p \rightarrow n\bar{K}^0$ implies no baryon exchanges of $\bar{10}$ or 27 multiplets. On this basis we might expect that the observed mesons with parity $(-)^J$ should belong to 1 or 8 representations, and

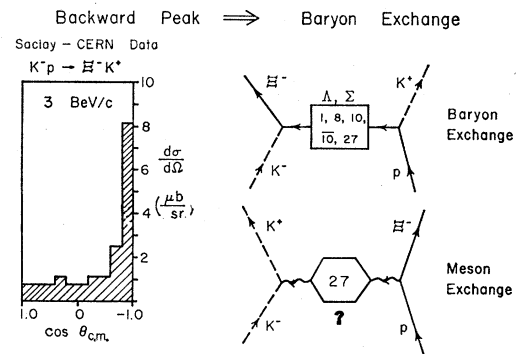


FIG. 5. Backward peak in the reaction $K^-p \rightarrow \Xi^-K^+$. [Data from J. Badier *et al.*, Saclay Report (1966).]

CERN and Wisconsin Data on
 Backward Elastic Scattering

at 3.5 BeV/c

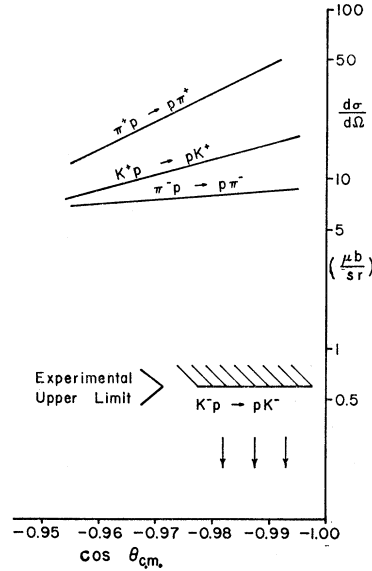
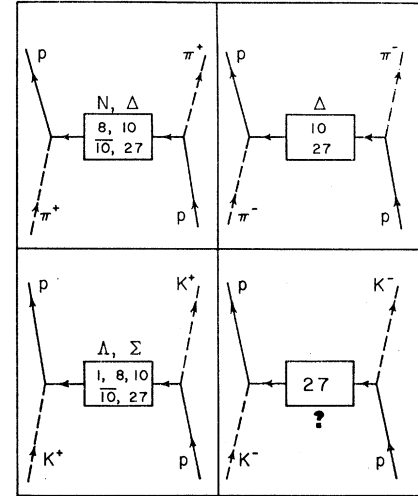


FIG. 6. Elastic scattering differential cross sections at backward angles. [Data from W. F. Baker *et al.*, Phys. Letters **23**, 605 (1966); J. Banaigs *et al.*, *ibid.* **24B**, 317 (1967); D. Cline, C. Moore, and D. Reeder, Phys. Rev. Letters **19**, 675 (1967).]

 Virtual Baryon Exchange Mechanisms
 for Backward Elastic Scattering


baryons should be classified as 1, 8, or 10 dimensional $SU(3)$ multiplets.¹

III. CLASSIFICATION OF FUNDAMENTAL PARTICLES

The classification of certain groups of particles with the same spin and approximately equal mass in $SU(3)$ multiplets has met with outstanding success. Such a classification system for the particles is considerably extended by the Regge theory which links particles with the same internal quantum numbers (I, Y, P , etc.) but with spin values that differ by two units ($\Delta J=2$). In this picture the particles are connected by a trajectory which represents the effective spin of the family in one of its real or virtual states. Associated with the trajectory is a new quantum number called "signature" which gives rise to the $\Delta J=2$ spacing rule for the physical particles on the trajectory. The signature (τ) is given by $\tau=(-)^J$ for mesons and $\tau=(-)^{J-1/2}$ for baryons.

A proposed classification scheme for the baryon resonances² which incorporates $SU(3)$ and Regge poles is shown on the following spin-mass (or Chew-Frautschi³) plot (Fig. 7). The 1, 8, and 10 $SU(3)$ multiplets are on horizontal planes of equal J . These multiplets have recurrences at intervals $\Delta J=2$ with increasing mass. If these ideas prove to be correct,

¹ These conclusions may not apply to particles whose exchange contributions are dynamically suppressed.

² V. Barger and D. Cline, Phys. Rev. **155**, 1792 (1967).

³ G. F. Chew and S. C. Frautschi, Phys. Rev. Letters **7**, 394 (1961).

then experimentalists may expect to find a multitude of yet undiscovered particles of high spin and large mass. If the trajectories continue to rise, then there is the exciting possibility that the number of particle recurrences on a given trajectory may actually be infinite!

Similar ideas have been applied to classify the meson resonances of high mass. Rather than discuss the proposed singlet and octet trajectory assignments for mesons, let us turn to the best studied example of meson trajectories—namely, the trajectory associated with the ρ -meson (Fig. 8). On the right-hand side of the plot in Fig. 8, the trajectory passes through the ρ meson at $J=1$ and further recurrences at $J=3, 5, \dots$, etc. The trajectory on the left side of the plot represents the "effective spin" of the exchange of this ρ meson family in a scattering process; the variable t is the 4-momentum transfer between the incoming and outgoing external mesons of the reaction.

IV. REGGE DESCRIPTION OF SCATTERING PROCESSES

The greatest utility of the Regge theory pertains to the peripheral exchange mechanism for scattering processes. The scattering amplitude f due to a meson Regge exchange has a characteristic phase and energy dependence—both of which are determined by the trajectory $\alpha(t)$.

$$f \sim -\gamma(t)$$

$$\times \left\{ \underbrace{[\exp(-i\pi\alpha) + \tau]}_{\text{phase factor}} / \sin \pi\alpha(t) \right\} \cdot \underbrace{(E_{\text{lab}}/E_0)^{\alpha(t)-1/2}}_{\text{energy dependence}}$$

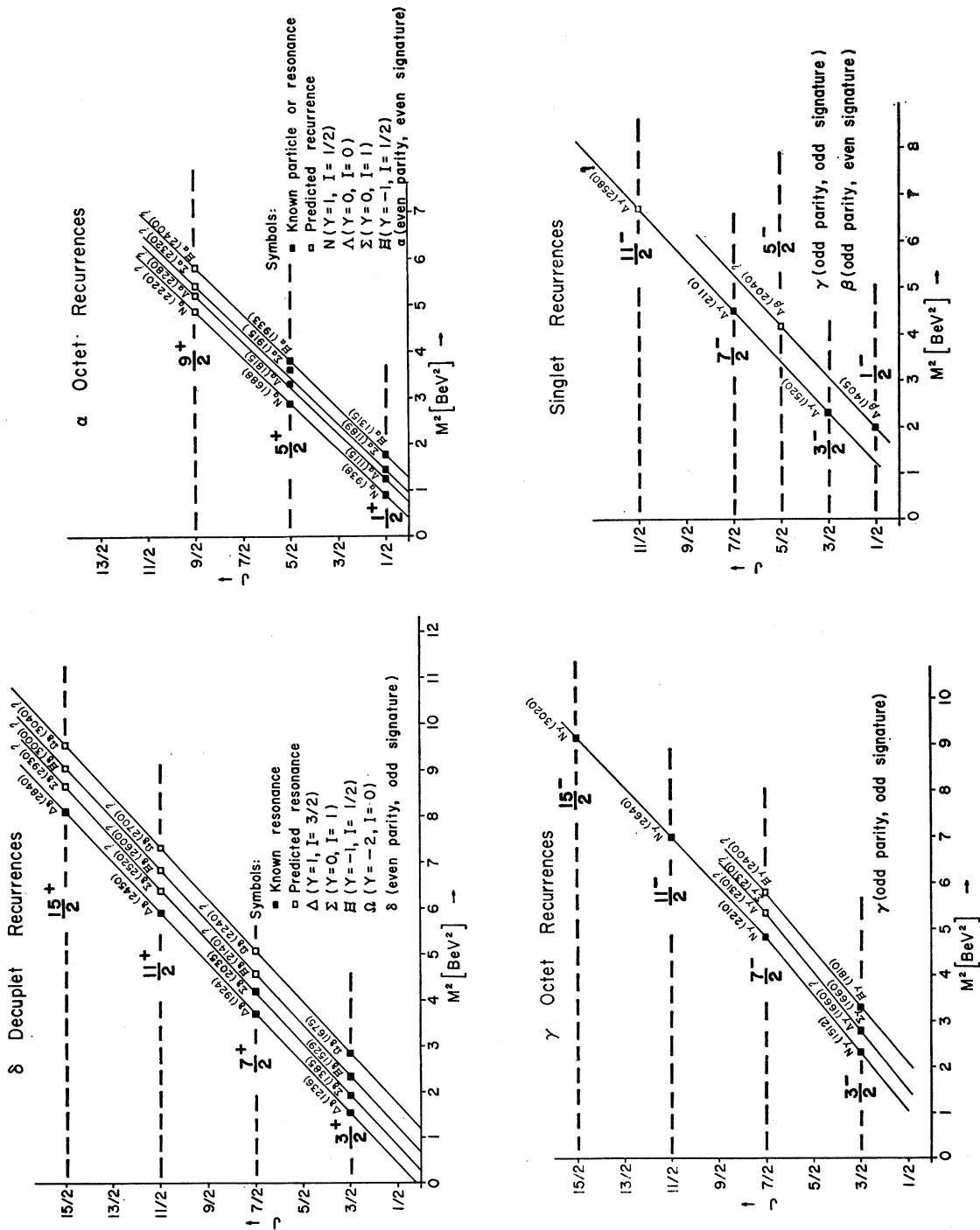
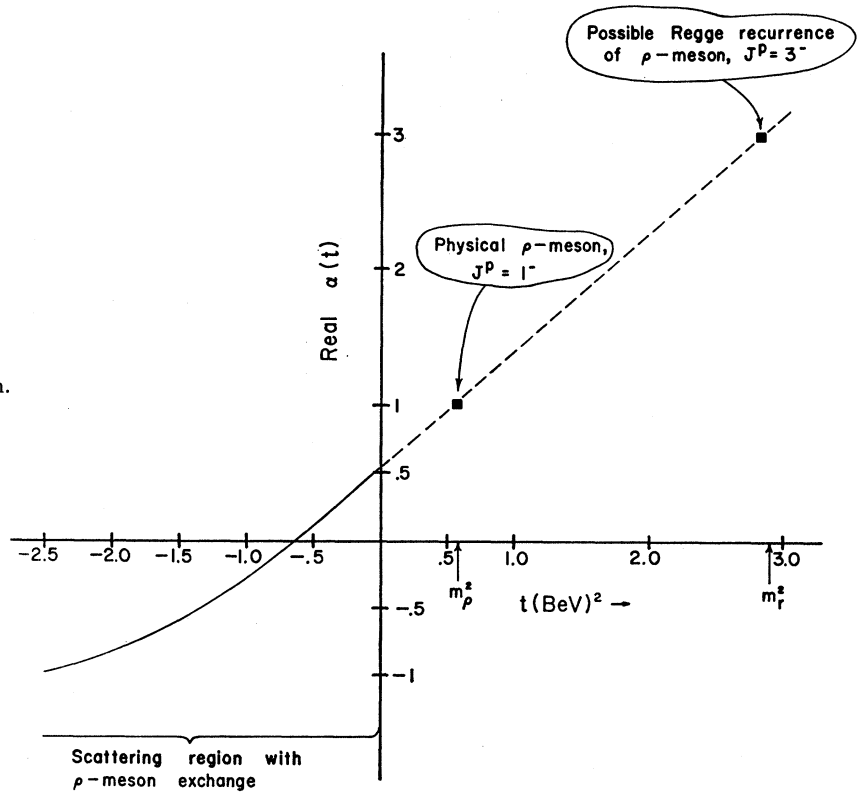


Fig. 7. Chew-Frautschi plots of baryon Regge recurrences classified according to 1, 8, and 10 representations of $SU(3)$. (Figure 15 of Ref. 2.)

FIG. 8. Regge trajectory of the ρ meson.



For the exchange of a single trajectory, the theory predicts a definite energy dependence, $d\sigma/d\Omega \sim (E_{lab})^{2\alpha(t)-1}$. For a linear trajectory at small t , we expect that the forward peak will shrink with energy like

$$\exp[-2|t|\alpha'(0)\ln(E_{lab}/E_0)].$$

These energy-dependent features seem to be completely consistent with all the high-energy data on the π^-p charge-exchange reaction which yield $\alpha_p(0) \sim \frac{1}{2}$, $\alpha_p'(0) \sim 1(\text{BeV}/c)^2$.

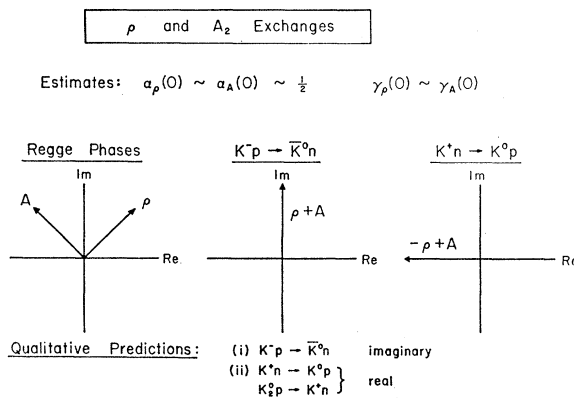


FIG. 9. Phase diagrams for ρ and A Regge amplitudes in KN and $\bar{K}N$ scattering.

The reaction $\pi^-p \rightarrow \pi^0n$ provided the first clear test of the Regge pole prediction for the phase of the ρ -exchange amplitude. Since $\tau = -1$ for the ρ trajectory, the prediction is

$$\text{Re} f / \text{Im} f = \tan[\pi\alpha_p(0)/2].$$

From the energy dependence of the differential cross

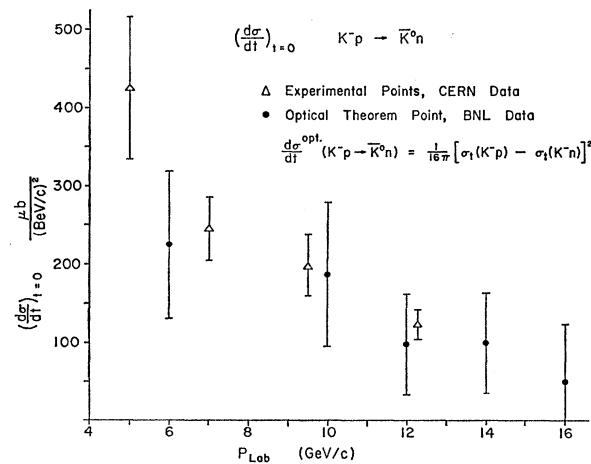
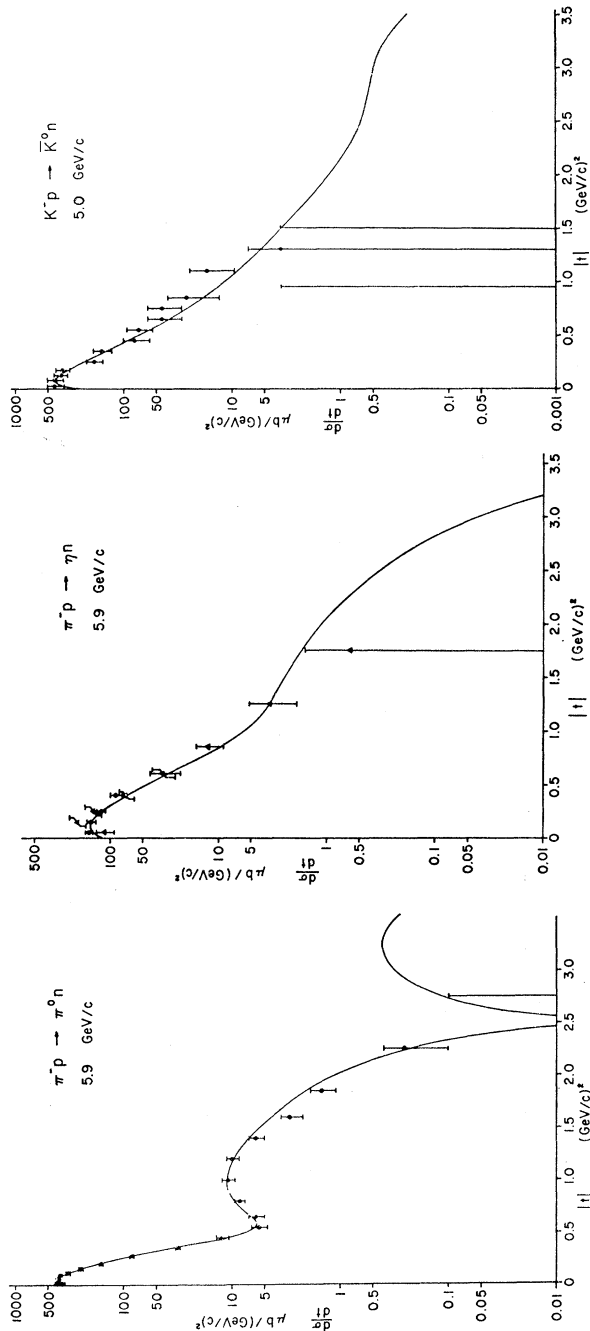


FIG. 10. Comparison of forward differential cross section measurements for $K^-p \rightarrow \bar{K}^0n$ with optical theorem values. The equality $(d\sigma/dt)_{t=0} \simeq (d\sigma/dt)_{optical}$ is expected in the ρ, A Regge exchange model. [Data from Fig. 1 of P. Astbury *et al.*, *Phys. Letters* 23, 396 (1966); and W. Galbraith *et al.*, *Phys. Rev.* 138, B913 (1965).]

FIG. 11. Representative fits to the $\pi^-p \rightarrow \pi^0n$, $\pi^-p \rightarrow \eta n$, and $K^-p \rightarrow \bar{K}^0n$ differential cross sections from a ρ , A Regge model. (Figure 1 of Ref. 5).



section, we have previously obtained $\alpha_\rho(0) \sim \frac{1}{2}$. Thus we expect $\text{Re } f / \text{Im } f \simeq 1$. The magnitude of this ratio can be directly determined from the data by the relation

$$\left| \frac{\text{Re } f}{\text{Im } f} \right|^2 = \frac{(d\sigma/dt)_{t=0}^{\text{observed}}}{(d\sigma/dt)^{\text{optical}}} - 1,$$

where $(d\sigma/dt)^{\text{optical}}$ is the contribution of $\text{Im } f$ to the differential cross section, as obtained from the optical theorem. Experimentally, this relation gives $|\text{Re } f / \text{Im } f| \simeq 1$, independent of energy as predicted.

The other familiar example of a single trajectory exchange occurs in the reaction $\pi^-p \rightarrow \eta n$. Here the Regge trajectory is associated with the A_2 meson, with $J^P = 2^+$, and the signature is $\tau = +1$. The energy dependence of this reaction gives $\alpha_A(0) \sim 0.4$. For $\alpha_A(0) \sim \frac{1}{2}$ we expect that $\text{Re } f / \text{Im } f \simeq -1$ for this scattering amplitude.

Some interesting qualitative predictions can be made for reactions in which both the ρ and A trajectories are exchanged. For example, the reaction $K^-p \rightarrow \bar{K}^0n$ is given by the combination $(\rho + A)$. For $\alpha_\rho \simeq \alpha_A$ and $\gamma_\rho \simeq \gamma_A$, the ρ and A Regge amplitudes are 90° out of phase⁴ (Fig. 9). Consequently, the $K^-p \rightarrow \bar{K}^0n$ scattering amplitude is predicted to be predominantly imaginary. Similarly, the reaction $K^+n \rightarrow K^0p$ is given by $(-\rho + A)$ and is predicted to be real. Recent measurements of $K^-p \rightarrow \bar{K}^0n$ at $t=0$ (Fig. 10) indicate that $(d\sigma/dt)^{\text{observed}} \simeq (d\sigma/dt)^{\text{optical}}$, as expected for a pure imaginary amplitude. High-energy measurements of $K^+n \rightarrow K^0p$ or $K_2^0p \rightarrow K^+n$ are desirable to further test the Regge phase predictions.

One can of course go much further than these qualitative predictions and analyze the differential cross sections with suitable parametrizations of the trajectory and residue functions. The next figure shows a representative example of such a fit to high-energy data on charge exchange reactions (Fig. 11). This particular analysis was carried out by Reeder and Sarma at Wisconsin.⁵ The dip in $\pi^-p \rightarrow \pi^0n$ at $t \simeq -0.6$ $(\text{BeV}/c)^2$ is expected from the spin dependence of the Regge amplitudes and occurs where the effective spin of the ρ trajectory goes through zero.⁶

V. SU(3) SYMMETRY FOR REGGE RESIDUES

In order realistically to incorporate $SU(3)$ symmetry predictions in the description of scattering processes, it is necessary to employ a suitable dynamical framework. Then symmetry breaking effects such as non-

⁴ Given $\alpha_\rho \simeq \alpha_A$, the relation $\gamma_\rho \simeq \gamma_A$ for the Regge residues can be empirically inferred from the approximate total cross section equality $\sigma_t(K^+p) \simeq \sigma_t(K^+n)$. The set of equalities $\alpha_\rho = \alpha_A$ and $\gamma_\rho = \gamma_A$ is known as "exchange degeneracy." See R. C. Arnold, Phys. Rev. Letters 14, 657 (1965); A. Ahmadzadeh, *ibid.* 16, 952 (1966).

⁵ D. D. Reeder and K. V. L. Sarma, Nuovo Cimento 51, A169 (1967).

⁶ F. Arbab and C. B. Chiu, Phys. Rev. 147, 1045 (1966).

degenerate masses or direct channel resonances can be taken into account. In the context of the Regge pole model, $SU(3)$ symmetry is normally applied to the residue of the Regge pole amplitude. Since the residue can be factored into parts associated with the vertices of the scattering amplitude, $SU(3)$ symmetry can be used at the vertices to relate the contributions of a given Regge pole in different processes. Symmetry breaking effects can always be taken into account by allowing nondegenerate masses for the external particles and nondegenerate trajectories for different Regge exchanges.

A particularly simple application of $SU(3)$ symmetry is provided by the meson-nucleon charge exchange reactions. Here the baryon vertex $p \rightarrow n$ is fixed (hence no arbitrariness is introduced through F/D ratios at the nucleon vertex). Further simplification results from the fact that there are only the two kinds of octet exchanges (with $I=1$ and G parity $= \pm 1$) in these reactions. For definiteness, we label these exchanges by ρ and A , corresponding to the trajectories previously discussed, but the argument is more general. $SU(3)$ symmetry at the meson vertex directly relates the four charge exchange scattering amplitudes to the ρ and A Regge amplitudes:

$$\begin{aligned} \langle \pi^- p | \pi^0 n \rangle &= -\sqrt{2}\rho; \\ \langle K^- p | \bar{K}^0 n \rangle &= \rho + A; \\ \langle K^+ n | K^0 p \rangle &= -\rho + A; \\ \langle \pi^- p | \eta n \rangle &= (\frac{2}{3})^{1/2} A. \end{aligned}$$

Thus we obtain two sum rules among the charge exchange reactions. One of these sum rules can be expressed in terms of total cross sections by use of the optical theorem⁷ (Fig. 12).

$$\begin{aligned} [\sigma_t(K^- p) - \sigma_t(K^- n)] - [\sigma_t(K^+ p) - \sigma_t(K^+ n)] \\ = [\sigma_t(\pi^- p) - \sigma_t(\pi^+ p)]. \end{aligned}$$

This sum rule for the total cross sections is in remark-

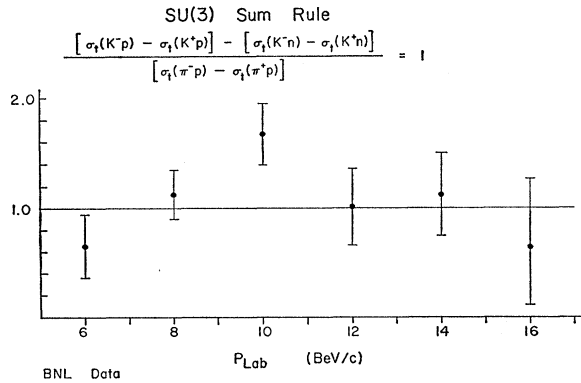


FIG. 12. Experimental evaluation of $SU(3)$ sum rule for total cross sections. Derivation of this sum rule requires only $SU(3)$ symmetric meson couplings for ρ exchange. (Figure 4 of Ref. 8).

⁷ V. Barger and M. H. Rubin, Phys. Rev. **140**, B1365 (1965).

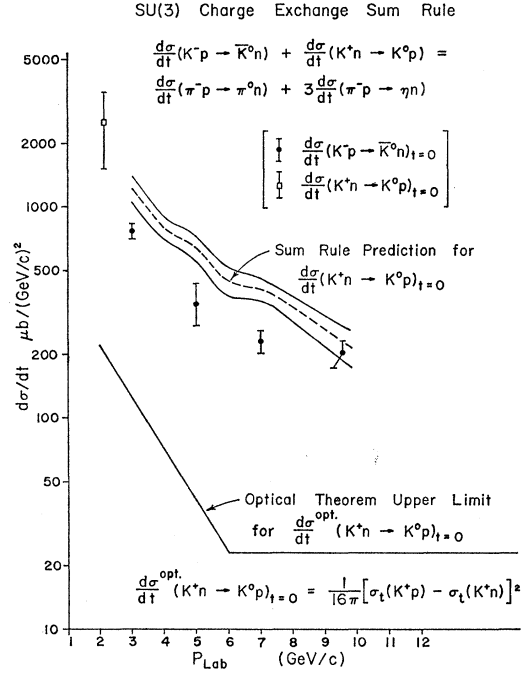


FIG. 13. Prediction of the $K^+ n \rightarrow K^0 p$ differential cross section from the $SU(3)$ charge exchange sum rule. (Figure 1 of Ref. 9).

ably good agreement with experiment.⁸ The other sum rule relates the four differential cross sections:

$$\begin{aligned} (d\sigma/dt)(K^- p \rightarrow \bar{K}^0 n) + (d\sigma/dt)(K^+ n \rightarrow K^0 p) \\ = (d\sigma/dt)(\pi^- p \rightarrow \pi^0 n) + 3(d\sigma/dt)(\pi^- p \rightarrow \eta n). \end{aligned}$$

The $K^+ n \rightarrow K^0 p$ scattering amplitude is predicted to be predominantly real from this sum rule, independent of any specific dynamical form of the exchange amplitudes⁹ (Fig. 13).

If we use the explicit forms of the ρ and A Regge amplitudes with independent residues at each vertex, a direct experimental test of the vertex symmetry can be made from an analysis of the data (Fig. 14). A least-squares fit to the six independent cross section combinations gives¹⁰

Analysis	Exact $SU(3)$
$\rho \bar{K} K / \rho \pi \pi = 1.12 \pm 0.12$	1
$A \bar{K} K / A \pi \eta = 1.07 \pm 0.15$	1

These results are consistent, within statistical errors, with exact symmetry for the ρ and A residues.

It has also been possible with Regge pole models to achieve very accurate fits to the high-energy data on all total cross sections¹¹ (Fig. 15). Such models are based

⁸ V. Barger and M. Olsson, Phys. Rev. **146**, 1080 (1966).

⁹ V. Barger and D. Cline, Phys. Rev. **156**, 1522 (1967).

¹⁰ V. Barger and M. Olsson, Phys. Rev. Letters **18**, 294 (1967).

¹¹ V. Barger and M. Olsson, Phys. Rev. Letters **16**, 545 (1966).

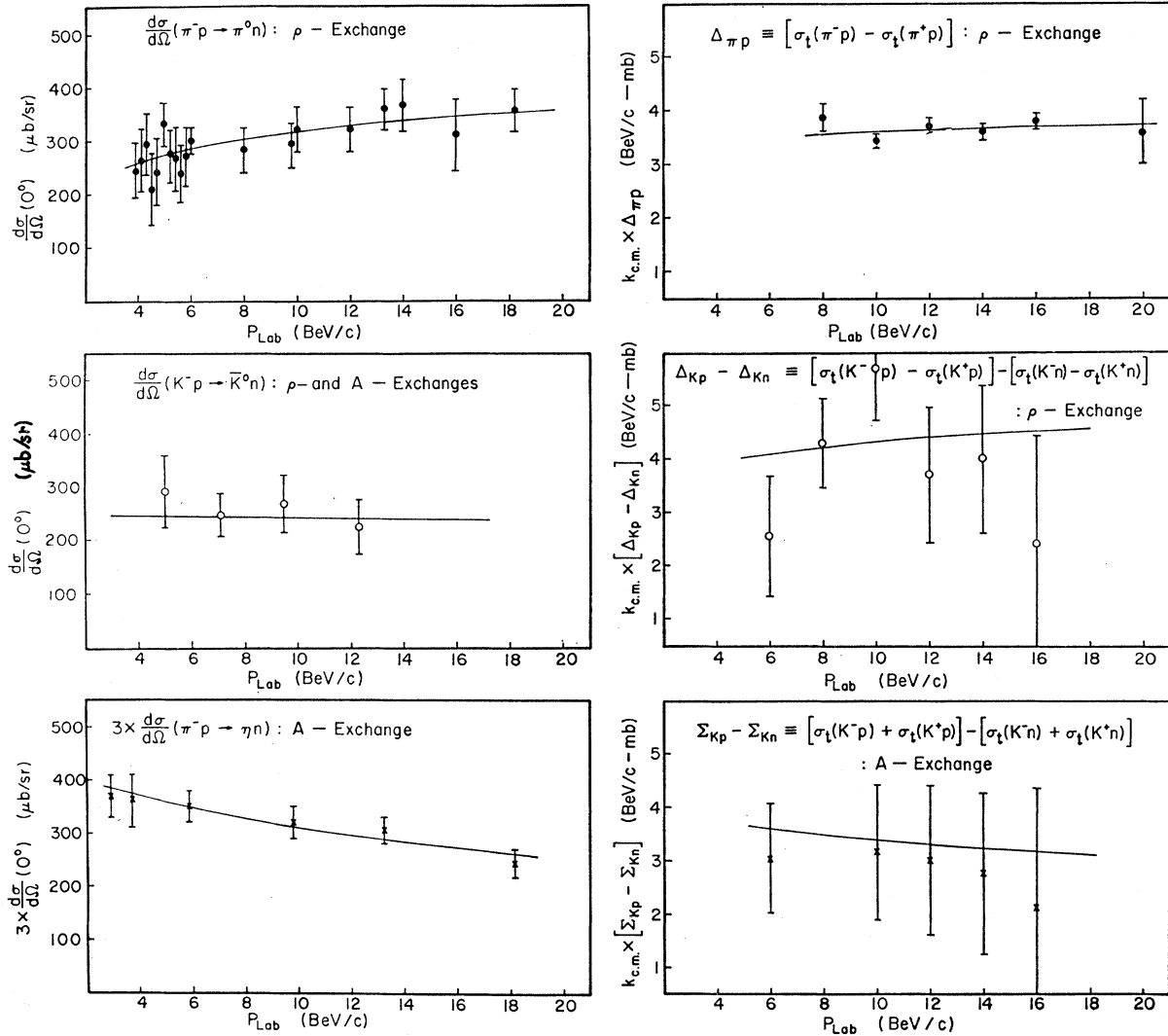


FIG. 14. Cross-section data used in testing the validity of $SU(3)$ symmetry for the ρ and A Regge residues. Solid curves represent the resultant Regge fits. (Figure 1 of Ref. 10.)

on exchanges of singlet and octet multiplets of mesons with $SU(3)$ symmetry for the vertices. The data show the smooth variation with energy expected in the Regge pole theory, but unfortunately the theoretical models are by no means unique.

VI. INTERFERENCE MODEL

Since the Regge pole model seems to provide a satisfactory description of the scattering at high momenta, a logical objective is to try to extend the model to the intermediate momentum range. To this end, an interference model has been proposed which takes into account the probability of resonance formation in the direct channel as well as the Regge exchange mechanism. To illustrate the interference

model, let us return to the $\pi^-p \rightarrow \pi^0n$ amplitude at the forward direction. The Regge ρ -exchange amplitude is already determined by the high-energy analysis. The direct channel resonance amplitude is calculated from a sum of Breit-Wigner amplitudes for the known πN resonances. The results of including both the Regge and resonance amplitudes are illustrated in the figure¹² (Fig. 16) for $[\sigma_t(\pi^-p) - \sigma_t(\pi^+p)]$. The dotted curve shows the ρ -exchange contribution alone. The solid curve includes both the resonance and Regge amplitudes. The $I = \frac{3}{2}$ resonances interfere destructively and the $I = \frac{1}{2}$ resonances constructively with the ρ -exchange amplitude. The interference model also accurately

¹² V. Barger and M. Olsson, Phys. Rev. 151, 1123 (1966).

describes the differential cross section for $\pi^-p \rightarrow \pi^0n$ near the forward direction.

Similar structure in the π^-p elastic scattering cross section at the backward direction has been interpreted in the framework of the interference model. Here the relevant Regge exchange amplitude is the $I = \frac{3}{2}$ member of the decuplet (i.e., the trajectory associated with the $N_{3,3}^*$ resonance at 1236 MeV) (see Fig. 17). Since the direct channel resonance contribution is to be evaluated at 180° , each of the Breit-Wigner forms contains a factor of $(-)^l$ where l is the orbital momentum of the resonance. Because of this factor, the nature of the interference is sensitive to the parities of the resonances [$P = (-)^{l+1}$]. The assignment of the resonances to

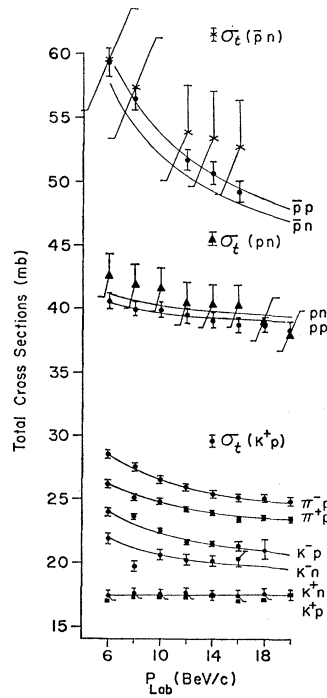


FIG. 15. Regge pole fits to total cross-section data at high energy. (Figure 1 of Ref. 11).

trajectories in a Chew-Frautschi plot (Fig. 18) fixes the parities.² For example, all the particles assigned to the trajectory of the $N_{3,3}^*$ must have positive parity. (Experimental spin-parity determinations exist only for the two lowest members of each trajectory.) Thus, the Regge spin-mass plot can be used to infer the parities of the resonances and hence to fix the signs of the Breit-Wigner amplitudes. At the same time we can extrapolate in the Chew-Frautschi plot to the value of the virtual (mass)² of the exchange, and thereby determine the effective spin α of the exchange. This value for α in turn fixes the phase and energy dependence of the Regge amplitude. Such interrelationship of the Regge exchange and direct channel resonance amplitudes places severe consistency conditions on the interference model calculations.

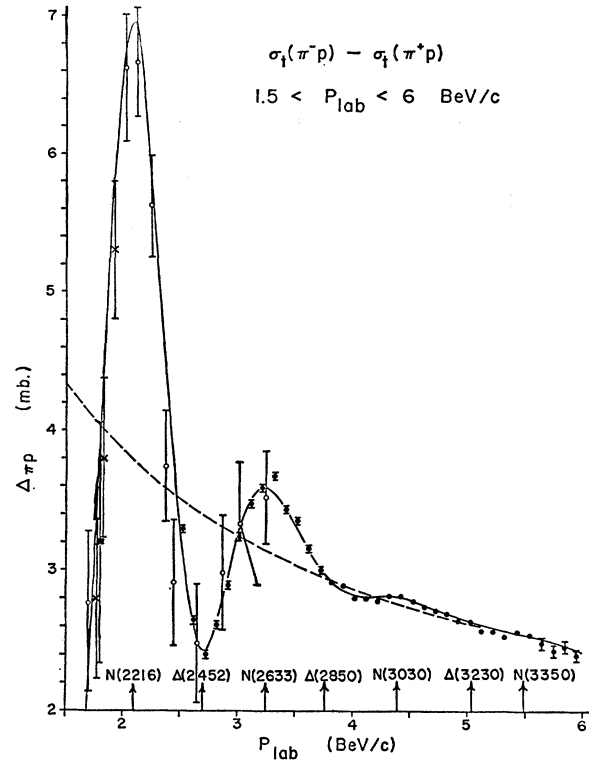


FIG. 16. Interference model fit to the total cross-section difference [$\sigma_t(\pi^-p) - \sigma_t(\pi^+p)$]. The dashed curve represents the contribution of the Regge ρ -exchange amplitude. (Figure 1 of Ref. 12).

The calculation of the 180° π^-p differential cross section from this model is shown in the figure² (see Fig. 19). The Regge amplitude accounts for essentially all of the cross sections above 5 BeV/c. The two decade valley near 2.1 BeV/c results from totally destructive interference between the Regge and resonance amplitudes. Changing the parities of individual resonances from the proposed recurrence assignments changes the interference pattern and destroys the agreement with experiment.

Since interference model calculations are sensitive to the quantum numbers of the direct channel resonances, this approach holds great promise for indirect

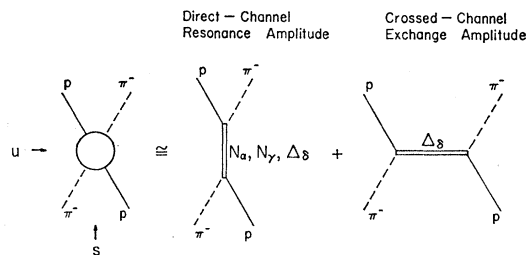


FIG. 17. Illustration of the interference model approximation for π^-p elastic scattering in the backward hemisphere. (Figure 1 of Ref. 2).

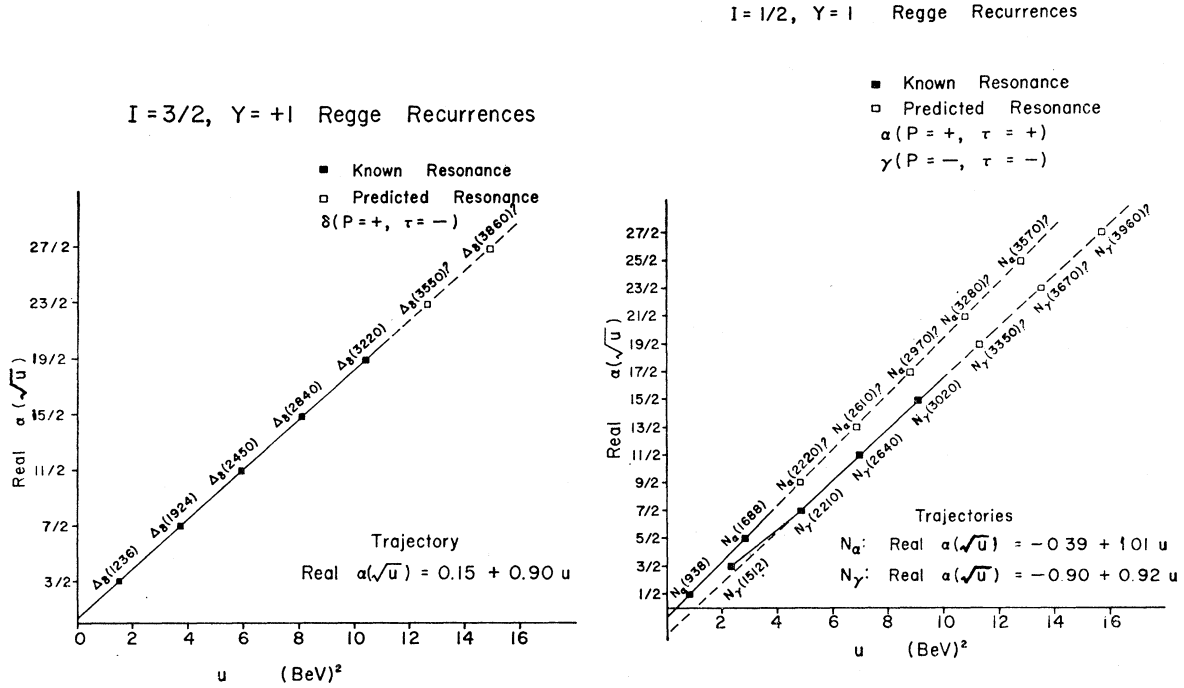


FIG. 18. Chew-Frautschi plot of the $Y = +1$ fermion resonances. (Figure 2 of Ref. 2).

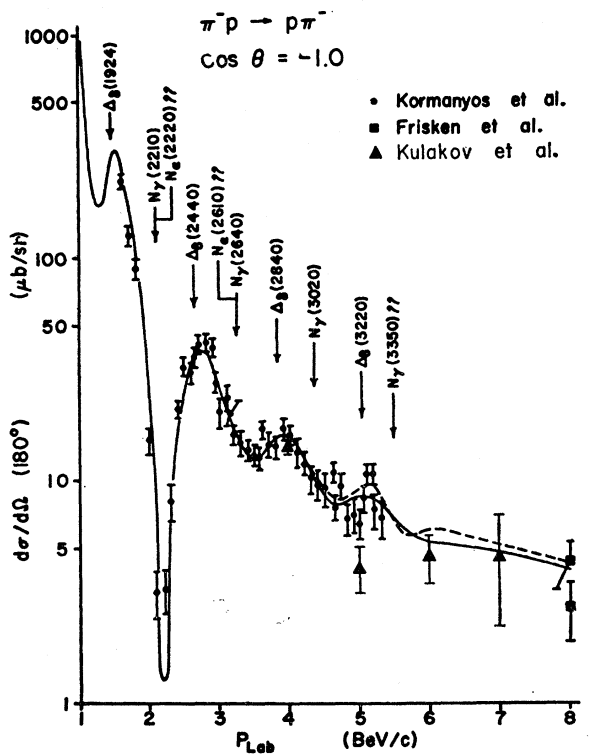


FIG. 19. Interference model calculation for the $180^\circ \pi^- p$ elastic scattering differential cross section as a function of laboratory momentum. (Modified version of Fig. 3 of Ref. 2.)

experimental studies of high-mass particles. *In fact, the interference model may eventually serve as the high-energy equivalent of low-energy phase-shift analyses.* Very accurate angular distributions as a function of energy and angle will be required for such studies. A three dimensional plot of the predicted structure of the $\pi^- p$ differential cross section shows the patterns to be expected (Fig. 20).

The Regge exchange amplitude plays a major role in these interference model calculations. Direct channel resonances alone do not provide the sizeable cross sections observed experimentally at high energies. A case in point is $K^- p$ elastic backscattering. In this

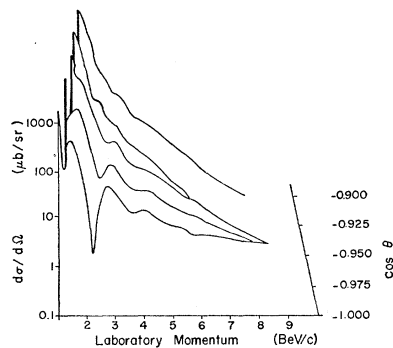


FIG. 20. Predicted structure in $\pi^- p$ backward elastic scattering as a function of both momentum and angle.

process a multitude of resonances contribute in the direct channel, but there is no Regge exchange. As a result, the experimental cross section for this process is an order of magnitude smaller than for the elastic processes which can proceed via baryon exchange (cf. Fig. 6).

VII. FUTURE PROSPECTS

As more data on backward scattering become available, $SU(3)$ predictions for the residues of the baryon exchange amplitude will be testable. One particularly simple equality (Fig. 21) that can be checked is

$$(d\sigma/d\Omega)(K^-p \rightarrow \Sigma^+\pi^-) = (d\sigma/d\Omega)(\pi^-p \rightarrow p\pi^-).$$

For backward scattering, both of these processes proceed via $I=\frac{3}{2}$, $Y=1$ baryon exchange. The predictions at $\cos \theta_{c.m.} = -1$ and $\cos \theta_{c.m.} = -0.95$ for $K^-p \rightarrow \Sigma^+\pi^-$ are shown by the solid and dotted curves, respectively.¹³ The few data points available are averages over the interval $-0.95 < \cos \theta < -1$. There are a variety of other such interesting $SU(3)$ relations which await the arrival of further data on backward scattering cross sections.

In summary, I have attempted to show a representative sample of experimental data to which Regge pole models have been applied with apparent success. Much work remains to be done, but the over-all picture is quite promising. The combination of the $SU(3)$ and Regge theories may lead to a systematic explanation of

¹³ V. Barger and D. Cline (unpublished).

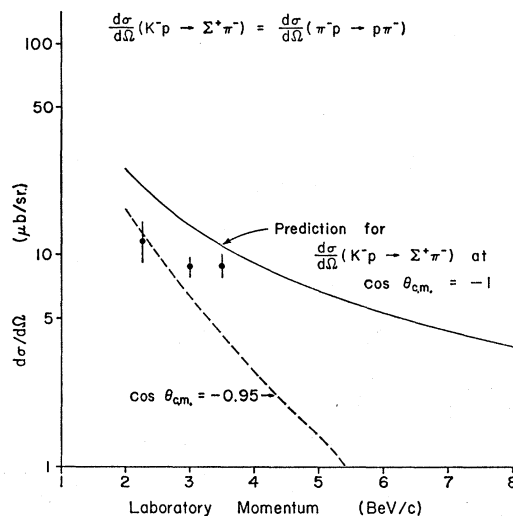


FIG. 21. Predicted differential cross section for the reaction $K^-p \rightarrow \Sigma^+\pi^-$ at backward angles. The prediction is based on $SU(3)$ symmetric residues for Δ_{δ} Regge exchange. The Δ_{δ} exchange contribution has been determined from an interference model analysis π^-p backward elastic scattering. (Refs. 2, 13.)

the data on the scattering of the fundamental particles and at the same time provide a basis for the classification of the increasing number of particle states.

ACKNOWLEDGMENTS

I thank Professor David Cline and Professor Martin Olsson for discussions and collaborations on many aspects of the material discussed in this paper.